Phase transition of prion protein initiates proteinase K resistant amyloid formation

Hiroya Tange[1,2], Daisuke Ishibashi[1], Takehiro Nakagaki[1], Yuzuru Taguchi[1], Yuji O Kamatari[3], Hiroki Ozawa[2] and Noriyuki Nishida[1]

1. Department of Molecular Microbiology and Immunology, Graduate School of Biomedical Sciences, Nagasaki University, Nagasaki, Japan

2. Department of Neuropsychiatry, Graduate School of Biomedical Sciences, Nagasaki University, Nagasaki, Japan

3. Center for Emerging Infectious Diseases, Gifu University, Gifu, Japan.

corresponding author: Hiroya Tange, Daisuke Ishibashi

Email: To whom correspondence should be addressed Hiroya Tange, bb55416003@ms.nagasaki-u.ac.jp or Daisuke Ishibashi, daishi@nagasaki-u.ac.jp

Keywords

Prion, Phase separation, ATPS, Amyloid

Author Contributions

Hiroya Tange conceived and planned the idea, designed the theory and experiment, collecting data, calculation, data analysis, interpretation and wrote the paper. Daisuke Ishibashi, Yuzuru Taguchi, Hiroki Ozawa and Noriyuki Nishida supervised on writing manuscript. Yuji O Kamatari performed FTIR analysis. Daisuke Ishibashi and Takehiro Nakagaki advised on experiments. All authors discussed the results and contributed to the final manuscript.

Author Summary

What initiates the sporadic misfolding process of PrP^{C} remains to be elucidated. Here, we show that rPrP undergoes LPS at the interface of ATPS of polyethylene glycol (PEG)/dextran; also, subsequent liquid–solid phase transition attributed to the maturation of β-sheet structure initiated the spontaneous conversion of rPrP into PrP^{Sc}-like amyloid. The intrinsically disordered region of PrP, residues 23–89, and kosmotropic anions were essential for the overall reaction. As the conversion of the protein proceeds without providing kinetic energy in this *in vitro* model, the findings suggest that LPS is associated with the occurrence of prion diseases and provide a new understanding of prion emergence.

Abstract

In prion diseases, the causative agent is thought to be solely composed of misfolded prion proteins (PrP^{Sc}). It has been shown that PrP^{Sc} can convert host-encoded normal isoform of prion protein (PrP^{C}), but the spontaneous emergence of PrP^{Sc} is still enigmatic. Certain amyloidogenic proteins have recently been shown to undergo liquid phase separation (LPS) and liquid–solid phase transition. These phenomena are now believed to play an important role in the initial step of pathological aggregation in neurodegenerative diseases. We investigated whether purified full-length human recombinant prion protein (rPrP, residues: 23–231) refolded normally can directly convert into PrP^{Sc}-like amyloid via LPS and subsequent phase transition. The proteins underwent LPS in an aqueous two-phase system (ATPS) composed of 9% polyethylene glycol (PEG; M.W. 6000) and 9% dextran (M.W. 180,000) with kosmotropic anions. The maturation of droplets could be monitored by microscopy because the droplets of rPrP were positively stained by thioflavin T (ThT) at the beginning of LPS. Notably, phase transition occurred within an hour, accompanied by the β-sheet transition of rPrP. The aged gels of rPrP acquired resistance to proteinase-K (PK) digestion and formed amyloids, as confirmed by Congo red staining. These overall reactions required the N-terminal region of PrP, amino acid residues 23–89, which is known as an intrinsically disordered region. Our results suggest that the aberrant phase transition may be associated with the sporadic emergence of prions, and our assay should be useful for understanding the *in vitro* generation of prions.

Introduction

Transmissible spongiform encephalopathies (TSEs), also called prion diseases, are infectious and fatal neurodegenerative diseases with rapidly progressive dementia, such as Creutzfeldt–Jakob disease, in humans (1). TSEs are characterized by the accumulation of misfolded prion proteins (PrP^{Sc}), which are cell surface glycoproteins expressed particularly in neurons and well preserved among mammalian species (2). In the protein-only hypothesis, host-encoded normal isoform of prion protein (PrP^{C}) converts into a disease-specific isoform, PrP^{Sc}, characterized by resistance to proteinase-K (PK) digestion (3,4). This conversion process presumably proceeds via the direct interaction between PrP^{C} and PrP^{Sc}, and PrP^{Sc} is supposedly the sole component of prions (5,6). The deposition of PrP^{Sc} leads to devastating neuronal cell death, resulting in characteristic spongiform changes in the brain (7). Several studies, including our own, have attempted to create artificial PrP^{Sc} from PrP^{C} *in vitro*. The amplification of PrP^{Sc} has been successfully demonstrated using intermittent ultrasonication on brain homogenate in prion diseases called protein misfolding cyclic amplification (PMCA) (8,9). We also showed the ultra-sensitive detection of PrP^{Sc} from CSF by amplifying the conversion of recombinant PrP (rPrP) using quaking-induced conversion (QuIC) (10). These lines of experimental evidence indicate that PrP^{C} can convert into PrP^{Sc} and form amyloid fibrils when PrP^{Sc} exists as a seed. However, the initial step of the spontaneous misfolding process from PrP^{C} to PrP^{Sc} in the absence of PrP^{Sc} remains to be elucidated. PrP^{C} is known to have an intrinsically disordered region (IDR) at the N-terminal region, which is called the octa-peptide region, composed of five repeats of proline- and glycine-rich sequences. IDRs have been indicated to drive the formation of membraneless organelles by LPS (11). Recently, FUS in familial amyotrophic lateral sclerosis and tau protein in

Alzheimer's disease have also been reported to have IDRs; these proteins initiate LPS and a subsequent phase transition driven by the molecular assembly of IDRs (12,13). Thus, the aberrant phase transition of amyloidogenic proteins may cause spontaneous protein misfolding. In this study, we examined whether rPrP undergoes LPS by using an aqueous two-phase system (ATPS). We found that rPrP undergoes LPS at the interface of polymer fractions, and phase transition is promoted in a short time. The aged gels of rPrP acquired PK resistance with a β-sheet-rich structure, suggesting that our *in vitro* assay can be a useful model to understand the molecular mechanism of the spontaneous generation of PrP^{Sc}.

Results

rPrP undergoes LPS in ATPS

In general, polymers such as polyethylene glycol (PEG)/dextran are used to induce LPS of proteins, expecting that polymer molecules work as clouding agents by the excluded volume effect (14). First, we attempted to promote LPS of the full-length of rPrP in a single polymer solution, as previously reported (15). However, rPrP did not undergo LPS but resulted in salting out with PEG/dextran at concentrations greater than 10% (w/v) (data not shown). We then attempted this with ATPS composed of PEG and dextran because the interface of the polymer may function like a cellular surface (16). We found that immediately after mixing 10 µM rPrP with PEG and dextran mixture containing sodium thiosulfate ($Na_2S_2O_3$), droplet formation could be observed at the interface of polymer fractions. Therefore, we postulated that the existence of the interface is an essential factor for the LPS of rPrP. To test this hypothesis, we performed investigations with combinations of various concentrations of polymers because the condition where ATPS could form an interface was clearly defined by the binodal curve (17) (Fig. 1A). We experimented with conditions below the binodal curve, with 0–4% (w/v) of each polymer (PEG/dextran); rPrP formed an amorphous aggregation and precipitated at the bottom of the well, but no droplet was observed (Fig. 1B). In contrast, under conditions above the binodal curve, with 6–9% (w/v) of each polymer (PEG/dextran), droplets suddenly appeared at the interface of the polymer fraction. Above the binodal curve, the polymer concentration is expected to be high enough to salt out rPrP, but rPrP was not salted out. As a result, the conditions for droplet formation corresponded to the binodal curve of ATPS, suggesting that the interface of ATPS was critical for rPrP droplet formation. The number of droplets changed in correlation with the concentrations of rPrP, suggesting that the droplets were composed of rPrP (Suppl. Fig. 1A, B). The droplets also formed in a manner dependent on the dose of $Na_2S_2O_3$ (Suppl. Fig. 1B). To confirm that the droplets consisted of rPrP, we performed examinations with Alexa 488-labeled rPrP and confirmed that the fluorescence was equally distributed in all of the droplets (Fig. 1C). We also found that the droplets could be stained by thioflavin T (ThT) immediately after their formation (Fig. 1D).

Kosmotropic anion species induce droplet formation

We next investigated the influence of salt type on droplet formation. Previous research reported that droplet size tended to be affected by kosmotropic salts (18). Thus, we next used various salts to identify the effect of the character of salt on LPS conditions. We hypothesized that kosmotropic anions may induce the assembly of rPrP molecules and promote LPS. Therefore, we investigated the effects of various sodium salts, such as NaCl, $Na_2S_2O_3$, Na_2CO_3, Na_2SO_4, and $Na_3C_6H_5O_7$. As expected, SO_4^{2-}, $C_6H_5O_7^{3-}$, and $S_2O_3^{2-}$ could induce droplet formation. The sizes of droplets with $Na_3C_6H_5O_7$ and Na_2SO_4 ranged from 5 to 10 µm, but they grew to around 50 µm with $Na_2S_2O_3$. The fluorescence intensity of droplets with $Na_3C_6H_5O_7$ and Na_2SO_4 was weak compared with $Na_2S_2O_3$ (Suppl. Fig. 2). Because the PrP-droplet formation was reproducible at 9% (w/v) of each polymer (PEG/dextran) with 120 mM $Na_2S_2O_3$, we adopted these conditions for the following experiments.

The droplets of rPrP undergo liquid–solid phase transition

To investigate the character of the droplets, we continuously observed their behavior. First, the fresh droplets could seamlessly fuse with each other while they were floating at the interface and were completely independent of the polymer fraction (Fig. 2A), suggesting that droplets were in

liquid phase and had different surface tension from PEG and dextran. Confocal microscopic observation revealed that rPrP immediately changed its distribution and turned into droplets at the interface upon the addition of 120 mM $Na_2S_2O_3$. In addition, PEG fluorescence colocalized in the droplets, suggesting that PEG bound to rPrP (Fig. 2B). Next, we analyzed fluorescence recovery after photobleaching of the droplets before and after incubation. Fresh droplets, formed immediately after LPS (0 min), showed full recovery of the intensity within 60 s, whereas the droplets incubated for 1 h at 37°C showed no recovery throughout the observation period (Fig. 3C, D). These findings suggest that the rPrP undergoes liquid–solid phase transition.

The N-terminal of PrPC (residues: 23–89) drives LPS and droplet maturation

The N-terminal region of PrP^C is known to be an IDR, whereas its C-terminal consists of a stable secondary structure with three α-helix regions, as revealed by NMR study (19). Under biological conditions, PrPC is not phosphorylated or methylated but is a GPI-anchored protein with two glycosylation sites (Fig. 3A). To determine whether IDRs of rPrP influence LPS, we first calculated its disordered propensity, hydrophobicity, and electric charge (Fig. 3B). The N-terminal of PrPC (residues: 23–111) is predicted to be an IDR by PrDOS (20). This region coincides with the positively charged region predicted by EMBOSS and hydrophilic region calculated from Protscale (21-23). Given the prediction results and the above findings, we hypothesized that the kosmotropic anion might enhance interactions between the N-terminal regions of the rPrP molecules by neutralizing their positive charges. To elucidate the role of the N-terminal region, we compared the behavior of rPrP and an N-terminal truncated mutant, rPrP Δ (23–89), in ATPS. As a result, rPrP Δ (23–89) failed to form droplets, and very weak ThT-positive particle-like precipitates were observed at the interface of the polymer fraction, whereas the droplet of rPrP increased fluorescence intensity over time (Fig. 3C, D). These precipitates of rPrP Δ (23–89) showed no increase in fluorescence intensity throughout the observation period up to 48 h (Fig. 3E). Interestingly, quantification of ThT fluorescence intensity showed that there was a significant difference between rPrP and rPrP Δ (23–89) from the beginning of the reaction (0 min) to the end of the observation period (48 h), suggesting that β-sheet conversion rapidly progressed via liquid–solid phase transition (Fig. 3F, G). Full-length mouse rPrP (Mo-rPrP, residues: 23–231) also showed similar results (Suppl. Fig. 3A–D). Thus, this phenomenon is not specific to human rPrP but may be universally applicable among species. Because the rapid growth of ThT fluorescence coincides with the timing of a liquid–solid phase transition (~1 h), we postulated that the droplets rapidly became insoluble and eventually matured to acquire properties of PrP^{Sc}. To verify this, we incubated droplets for 30 min and collected them by centrifugation from the P1 fraction. The gels in the P1 fraction, which is a sequential product of droplets, were ThT-positive and did not dissolve in dH_2O (Fig. 4A). These gels remained stable for months (not shown). To investigate the insolubility, we resuspended the gels in the P1 fraction with 1% sarkosyl and reprecipitated them by centrifugation as the P2 fraction. Western blot analysis showed that the gels were insoluble against sarkosyl (Fig. 4B). As for the negative control, namely, samples without the salt (rPrP: dH_2O) containing no droplet, all of the rPrP could be recovered from the supernatant, and quantification of band intensity showed no significant difference between with and without sarkosyl (Fig. 4C). Next, we examined whether these gels acquire PK resistance. We digested gels aged for 72 h and incubated with PK. Surprisingly, the appearance of aged gels remained unchanged after PK digestion (Fig. 4D). SDS-PAGE and western blotting of the aged gels collected by centrifugation showed that the aged droplets certainly contained oligomers of rPrP (Fig. 4E). Quantification of band intensity showed that 40% of rPrP remained undigested (Fig. 4F). A small PK-resistant fragment with a band shift could be seen around 10–15 kDa, resembling the PMCA product from another study (24). The existence of the polymers or the salt did not affect the efficiency of PK digestion. We further attempted to confirm that the rPrP in the droplets was amyloid. The aged gels were stained with Congo red but did not show apple-green birefringence under cross-polarized light (Fig. 4G). FTIR analysis showed that the aged gels had a distinctive peak at 1620 cm^{-1} in the β-sheet region of second-derivative spectra, which shifted from 1651 cm^{-1} in the α-helix region from the native form of rPrP (Fig. 4H). These results suggest

that rPrP converted into β-sheet-rich amyloid inside the droplets and acquired insolubility and PK resistance.

Discussion

Here, we demonstrated that rPrP could undergo LPS under the conditions above the binodal curve of ATPS and that the aged gels became β-sheet-rich, PK-resistant amyloid through liquid–solid phase transition. Notably, IDR, the N-terminal region of PrP^C (residues: 23–89), was shown to be essential for the overall reaction. The uniqueness of our study is that the conversion processes proceed without the provision of kinetic energy, unlike PMCA and RT-QUIC (8-10). The interface of ATPS and the kosmotropic anions possibly provided the optimal environment for the reaction.

ATPS has been used for a wide range of purposes such as purification of enzymes, nucleic acids, and viruses by providing a gentle environment for biomolecules and stabilizing their structure (17,25). The effects of various salts on the purification by ATPS have been well documented. For example, salt changes the distribution of monomeric IgG into the PEG fraction, whereas aggregated IgG remains in the dextran fraction (26). Kosmotropic anions are reported to enhance the migration of positively charged proteins to the PEG-enriched fraction (27). Thus, kosmotropic anions may affect the N-terminal region of rPrP because this region is positively charged, as shown above (Fig. 3A). Furthermore, PEG has no significant direct effect on the conversion reaction of PK-resistant PrP (28). Thus, the combination of ATPS and kosmotropic anions induced LPS of rPrP, whereas the native structure of rPrP was stabilized and polymers worked as appropriate crowding agents.

Regarding the effect of the interface, the interface of PEG and dextran was indispensable for LPS of rPrP because the droplets of rPrP appeared exclusively in the conditions above the binodal curve of ATPS. The interface of ATPS may have similar effects as the air/water interface, which reportedly plays an important role in other *in vitro* amyloid formation methods by partially denaturing protein molecules to make them prone to aggregation (29-31). Furthermore, a similar study showed that dsDNA and actin fiber are differently distributed inside the dextran phase, which is called cell-sized aqueous microdroplets (CAMD), providing cell-like crowded microenvironments (32). Therefore, the interface of PEG/dextran can be regarded as a cellular membrane having different crowding conditions imitating the intra/extracellular environment.

However, under physiological conditions, PrP^C reportedly interacts with various macromolecules such as RNA and lipids (33-35). These molecules may enhance the efficiency of LPS because these previous reports demonstrated that Aβ-oligomer and DNA-aptamer drive a liquid–solid phase transition of PrP through the interaction of residues 95–110 and 90–120 (15,36). Consistent with recent studies showing that LPS may participate in spontaneous amyloid formation of FUS and Tau, our data suggest that the aberrant phase transition of protein may initiate the pathogenesis of neurodegenerative diseases (12,13). In the process of liquid-to-solid transition, IDR assembles protein molecules and forms a cross-β structure comprising stacks of short β-strands (37). The N-terminal region of PrP^C, which is composed of five repeats of an octa-peptide region (PHGGGWGQ), may form a cross-β structure inside droplets. Previous research showed that the length of IDRs is related to the incubation period and protease resistance; furthermore, amyloid fibrils from the N-terminal region (residues: 23–144) are reportedly infectious in mice (38-40). Therefore, the N-terminal region of PrP plays an important role in infectious amyloid formation. Thus, the possible conversion process via LPS is that (i) the N-terminal region with a positive charge is neutralized by kosmotropic anion, inducing the direct interaction of dipole (G,Q) and π-π stacking (W) of the octa-peptide region to form a short cross-β sheet structure (41), (ii) the maturation process starts from the N-terminal region, followed by the conversion of the C-terminal region resulting in oligomerization of the β-sheet structure inside droplets. This process may be similar to the *in silico* calculation model of conversion (42) (Fig 5A, B). However, further investigation is required on how the β-sheet structure acquires PK resistance.

In conclusion, we show that a liquid–solid phase transition converts rPrP into PrP^{Sc}-like amyloid *in vitro*. Our assay is kinetic-energy-free, quantifiable, and visualizes the conversion process over time. Further study should provide new insight to understand the spontaneous occurrence of PrP^{Sc} and a possible way to develop a new quick detection method for prions; ATPS will be useful to analyze the LPS of other membrane proteins.

Materials and Methods

Protein expression and purification

We prepared three rPrPs: full-length human PrP (residues: 23–231), truncated human PrP (residues: 90–231), and Mo-rPrP (residues: 23–231). All constructs were expressed in Escherichia. coli strain DH5α. Expression and purification were performed as previously described (10,43). After purification, each protein solution was frozen at −80°C with a 150 µl aliquot and thawed for single use. For use in the experiment, each protein solution was centrifuged at 15,000 rpm for 10 min at room temperature (RT) before use. To prepare labeled protein, Alexa Fluor 488 Microscale Protein Labeling Kit (Invitrogen, A30006) was used. The procedure was performed in accordance with the manufacturer's instructions.

Disorder propensity and charge prediction

Disorder propensity was calculated using PrDOS (18), and charge prediction was performed using EMBOSS (19,20). The amino acid sequence from Uniprot (P04156) was used.

Droplet formation assay (polymer and salt solution preparation)

Polymer solutions were prepared from PEG (M.W. 6000) (Wako) and dextran (M.W. 180,000) (Nacalai Chemical). Each component was dissolved with dH_2O and prepared as 50% (w/v) PEG and 25% (w/v) dextran, with storage at 4°C with a 1 ml aliquot. We created a phase diagram by direct observation of polymer droplets using differential interference contrast (DIC) microscopy. PEG-dextran polymer solutions were prepared as 20 µl of solution at concentrations ranging from 1% to 10% (w/v) of each polymer (PEG/dextran). The polymer solutions were vigorously vortexed, and 5 µl of the solution was loaded onto a slide glass, after which the images were acquired. For confocal microscopy observation with fluorescence, 0.01% rhodamine-PEG (Nanocs, PG1-RB-5k) was used. To prepare salt solutions, we made 2 M stocks of NaCl, $Na_2S_2O_3$, Na_2SO_4, $NaHCO_3$, and $Na_3C_6H_5O_7$, all purchased from Wako and Nacalai Chemical. Each solution was stored at RT.

To make ATPS solution, each polymer solution was mixed at concentrations ranging from 1.5% (w/v) to 13.5% (w/v) with 25 to 200 mM salt (final: 1–9% (w/v) of each polymer, PEG/dextran with 15 to 120 mM salt). Then, the solution was pipetted well with vigorous vortexing to homogeneity. Experiments were performed on a scale of 50 µl (52.6 µl with ThT); 30 µl of ATPS solution was taken and 2.6 µl of 1 mM ThT (final concentration: 50 µM) was added. Next, 20 µl of rPrP solution (final concentration: 2–13 µM) was added to ATPS solution and gently pipetted 10–15 times. The entire solution was applied to a slide glass or 96-well plate (Thermo: 165305) for microscopic observation. Droplet observation was performed by confocal microscopy (LMS700; Carl Zeiss) and DIC microscopy (Axioskop2; Carl Zeiss). To evaluate ThT fluorescence, Colibri 7 was used as a luminous source at a wavelength of 485 nm. For droplet aging, the samples were applied to a 96-well plate or Eppendorf tube incubated at 37°C from 30 min to 72 h. All experiments were performed in triplicate.

Congo red staining

The samples were aged for 72 h at 37°C in ATPS solution, supplemented with 200 µl of dH_2O, and pipetted well. The aged gels were collected by centrifugation at 15,000 rpm for 10 min at RT and were stained with 50 µl of 1% Congo red (Aldrich: C8,445-3) solution for 30 min in an Eppendorf tube at RT. After staining, the sample was centrifuged under the same conditions again, after which the supernatant was discarded. The pellet was washed with 50 µl of dH_2O by pipetting, centrifuged again under the same conditions, and the supernatant was discarded. The pellet was suspended in 20 µl of dH_2O, and 5 µl was applied on a slide glass, followed by sealing with a cover glass. Microscopic observation was performed by confocal microscopy (Nikon) with a polarization filter. Images were acquired using NIS-Elements C software.

Fluorescence after photobleaching assay
FRAP was performed using LMS700 (Zeiss). Alexa488-labeled human rPrP was diluted 1:18 with native human rPrP. Bleaching was performed with 100% transmission of a 405, 488, or 500 nm laser. Pre-bleaching images were taken for 3 s (1 s frame rate, 3 frames), whereas post-bleaching images were acquired for the following 120 s (1 s frame rate, 120 frames) and analyzed with ZEN. The sizes of the bleached area and the background area were set in the first experiment. For each image, the bleached region and background region were calculated by ZEN, and the background was subtracted during analysis.

Sarkosyl treatment and proteinase K treatment
Sarkosyl and PK were purchased from Sigma-Aldrich. For sarkosyl treatment, the sample was incubated in ATPS solution at 37°C for 30 min, and 200 µl of dH_2O was added to the sample and pipetted well. The entire solution was centrifuged at 15,000 rpm for 10 min at RT. Supernatant-1 (S1) and Pellet-1 (P1) were collected. P1 was resuspended with 25 µl of dH_2O or 1% sarkosyl and then incubated at 37°C for 10 min. After incubation, samples were centrifuged at 15,000 rpm for 30 min at RT, and then Supernatant-2 (S2) and Pellet-2 (P2) were retrieved. PK solution was prepared as 10 µg/ml diluted with dH_2O. The samples were incubated at 37°C for 72 h in an Eppendorf tube. As a negative control, the solution containing the same amount of rPrP was treated with PK solution. The samples and PK solution were mixed by pipetting, applied to a 96-well plate, and incubated at 37°C. Observation with DIC microscopy was performed at the beginning of the reaction (0 min) and the end of incubation (30 min). Samples were retrieved from the 96-well plate, and each well was washed with 100 µl of dH_2O. The entire sample was collected in an Eppendorf tube and centrifuged at 15,000 rpm for 10 min at RT. The supernatant and pellet were collected. In both experiments, the supernatant was denatured with 6× SDS sample buffer (50 mM Tris-HCl pH 6.8, 5% glycerol, 1.6% SDS, 100 mM dithiothreitol); the pellet was then resuspended with 1× SDS buffer and boiled at 95°C for 10 min for SDS-PAGE.

Immunoblotting
Samples were applied to 18% acrylamide gel for SDS-PAGE and then transferred to a PVDF membrane. This membrane was blocked using 5%(w/v) skim milk with TBST (10 mM Tris-HCl pH 7.8, 100 mM NaCl, 0.1% Tween 20) at RT for 1 h. To detect PrP, the membrane was incubated with primary antibody R20 (1:1000) (44) diluted with 1% skim milk for 1 h at RT. Horseradish peroxidase-conjugated anti-rabbit IgG (1:10,000, GE Healthcare Life Sciences) was used as the secondary antibody. Protein bands were visualized using Clarity Western ECL substrate (Bio-Rad). Band intensity was measured and quantified by ImageJ.

Quantifying ThT fluorescence
Fluorescence intensity was quantified with FLUOstar Omega (BMG Labtech) in a 96-well plate with a spiral scan. The 96-well plate was covered with sealing tape (Greiner, J676060), incubated at 37°C, and monitored by the bottom reading of the fluorescence intensity every hour up to 48 h by using monochromators or filters with wavelengths of 448 nm excitation and 482 nm emission.

FITR analysis
Fourier transform infrared spectroscopy (FTIR) spectra were measured with a JASCO FT/IR-4700ST with attenuated total reflection. Five microliters of the sample was loaded on the grid. To prepare the sample for FTIR, we made 30× concentrated sample (aged for 72 h) from 1.5 ml scale to 50 µl. Aged gel was collected by centrifugation, as described above, and suspended in dH_2O.

Acknowledgments

We would like to thank Matsuo Atsuko, Hirono Nakata, Ren Matsushima for technical assistance, Toshiyuki Tsurumoto and Ryoichi Mori for polarized light microscopy observation. We would like to thank Enago (www.enago.jp) for the English language review. This research was supported by JSPS KAKENHI Grant number JP19K22600 and Sasakawa Scientific Research Grant from The Japan Science Society.

References

1. Prusiner S. B., Prions. Proc. Natl. Acad. Sci. U.S.A. 95, 13363–13383 (1998)
2. X. Roucou, M. Gains, A. C. LeBlanc, Neuroprotective Functions of Prion Protein. J. Neurosci. Res. 75, 153–161 (2004).
3. S. B. Prusiner, et al., Scrapie prions aggregate to form amyloid-like birefringent rods. Cell 35, 349–358 (1983).
4. J. Safar, et al., Eight prion strains have PrPSc molecules with different conformations. Nat. Med. 4, 1157–1165 (1998).
5. Prusiner SB (1991) Molecular biology of prion diseases. Science 252(5012):1515–1522.
6. F. E. Cohen, S. B. Prusiner, Pathologic Conformations of Prion Proteins. Annu. Rev. Biochem. 67, 793–819 (1998).
7. G. G. Kovacs, H. Budka, Prion diseases: From protein to cell pathology. Am. J. Pathol. 172, 555–565 (2008).
8. G. P. Saborio, B. Permanne, C. Soto, Sensitive detection of pathological prion protein by cyclic amplification of protein misfolding. Nature 411, 810–813 (2001).
9. J. Castilla, et al., Cell-free propagation of prion strains. EMBO J. 27, 2557–2566 (2008).
10. R. Atarashi, et al., Ultrasensitive human prion detection in cerebrospinal fluid by real-time quaking-induced conversion. Nat. Med. 17, 175–178 (2011).
11. Y. Shin, C. P. Brangwynne, Liquid phase condensation in cell physiology and disease. Science 357, eaaf4382 (2017)
12. A. Patel, et al., A Liquid-to-Solid Phase Transition of the ALS Protein FUS Accelerated by Disease Mutation. Cell 162, 1066–1077 (2015).
13. S. Wegmann, et al., Tau protein liquid–liquid phase separation can initiate tau aggregation. EMBO J. 37, 1–21 (2018).
14. A. A. Hyman, C. A. Weber, F. Jülicher, Liquid-Liquid Phase Separation in Biology. Annu. Rev. Cell Dev. Biol. 30, 39–58 (2014).
15. Kostylev, M. A. et al. Liquid and Hydrogel Phases of PrP C Linked to Conformation Shifts and Triggered by Alzheimer's Amyloid-β Oligomers. Mol. Cell 72, 426-443.e12 (2018).
16. E. Article, et al., Chemical Science A new design for an artificial cell: polymer microcapsules with addressable inner compartments that can harbor biomolecules, colloids or microbial species. 6893–6903 (2017).
17. M. Iqbal, et al., Aqueous two-phase system (ATPS): an overview and advances in its applications. Biol. Proced. Online 18, 1–18 (2016).
18. P. Mohammadi, et al., Controllable coacervation of recombinantly produced spider silk protein using kosmotropic salts. J. Colloid Interface Sci. 560, 149–160 (2020).
19. R. Zahn, et al., NMR solution structure of the human prion protein. Proc. Natl. Acad. Sci. U. S. A. 97, 145–150 (2000).
20. T. Ishida, K. Kinoshita, PrDOS: Prediction of disordered protein regions from amino acid sequence. Nucleic Acids Res. 35, 460–464 (2007).
21. P. Rice, L. Longden, A. Bleasby, EMBOSS: The European Molecular Biology Open Software Suite. Trends Genet. 16, 276–277 (2000).
22. E. Gasteiger et al., ExPASy: The proteomics server for in-depth protein knowledge and analysis. Nucleic Acids Res. 31, 3784–3788 (2003).
23. Sweet RM, Eisenberg D. Correlation of sequence hydrophobicities measures similarity in three-dimensional protein structure. J Mol Biol. 1983;171(4):479–488.
24. F. Wang, et al., Self-propagating, protease-resistant, recombinant prion protein conformers with or without in vivo pathogenicity. PLoS Pathog. 13, 1–23 (2017).
25. J. Benavides, M. Rito-Palomares, J. A. Asenjo, Aqueous Two-Phase Systems. Compr. Biotechnol. Second Ed. 2, 697–713 (2011).
26. C. Shibata, K. Iwashita, K. Shiraki, Selective separation method of aggregates from IgG solution by aqueous two-phase system. Protein Expr. Purif. 161, 57–62 (2019).

27. C. Shibata, K. Iwashita, K. Shiraki, Salt-containing aqueous two-phase system shows predictable partition of proteins with surface amino acids residues. Int. J. Biol. Macromol. 133, 1182–1186 (2019).
28. G. S. Baron, K. Wehrly, D. W. Dorward, B. Chesebro, B. Caughey, Conversion of raft associated prion protein to the protease-resistant state requires insertion of PrP-res (PrPSc) into contiguous membranes. EMBO J. 21, 1031–1040 (2002).
29. J. Dorosz, R. Volinsky, E. Bazar, S. Kolusheva, R. Jelinek, Phospholipid-induced fibrillation of a prion amyloidogenic determinant at the air /water interface. Langmuir 25, 12501–12506 (2009).
30. K. Sankaranarayanan, A. Dhathathreyan, J. Krägel, R. Miller, Interfacial viscoelasticity of myoglobin at air/water and air/solution interfaces: Role of folding and clustering. J. Phys. Chem. B 116, 895–902 (2012).
31. V. Sluzky, J. A. Tamada, A. M. Klibanov, R. Langer, Kinetics of insulin aggregation in aqueous solutions upon agitation in the presence of hydrophobic surfaces. Proc. Natl. Acad. Sci. U. S. A. 88, 9377–9381 (1991).
32. N. Nakatani, et al., Specific spatial localization of actin and dna in a water/water microdroplet: Self-emergence of a cell-like structure. ChemBioChem 19, 1370–1374 (2018).
33. N. R. Deleault, R. W. Lucassen, S. Supattapone, RNA molecules stimulate prion protein conversion. Nature 425, 717–720 (2003).
34. N. Sanghera, T. J. T. Pinheiro, Binding of prion protein to lipid membranes and implications for prion conversion. J. Mol. Biol. 315, 1241–1256 (2002).
35. N. R. Deleault, et al., Isolation of phosphatidylethanolamine as a solitary cofactor for prion formation in the absence of nucleic acids. Proc. Natl. Acad. Sci. 109, 8546–8551 (2012).
36. C. O. Matos, et al., Liquid-liquid phase separation and fibrillation of the prion protein modulated by a high-affinity DNA aptamer. FASEB J. n/a, 1–21 (2019).
37. Kato M, et al. Cell-free formation of RNA granules: Low complexity sequence domains form dynamic fibers within hydrogels. Cell. 2012; 149:753–767.
38. R. A. Moore, Octapeptide repeat insertions increase the rate of protease-resistant prion protein formation. Protein Sci. 15, 609–619 (2006).
39. A. Lau, et al., Octarepeat region flexibility impacts prion function, endoproteolysis and disease manifestation. EMBO Mol. Med. 7, 339–356 (2015).
40. J. K. Choi, et al., Amyloid fibrils from the N-terminal prion protein fragment are infectious. Proc. Natl. Acad. Sci. U. S. A. 113, 13851–13856 (2016).
41. C. P. Brangwynne, P. Tompa, R. V Pappu, Polymer physics of intracellular phase transitions. Nat. Phys 11, 899–904 (2015).
42. G. Spagnolli, et al., Full atomistic model of prion structure and conversion. PLoS Pathog. 15, 1–18 (2019).
43. Y. Miyazaki, T. Ishikawa, Y. O. Kamatari, T. Nakagaki, H. Takatsuki, Identification of Alprenolol Hydrochloride as an Anti-prion Compound Using Surface Plasmon Resonance Imaging. 367–377 (2019).
44. B. Caughey, G. J. Raymond, D. Ernst, R. E. Race, N-terminal truncation of the scrapie-associated form of PrP by lysosomal protease(s): implications regarding the site of conversion of PrP to the protease-resistant state. J. Virol. 65, 6597–603 (1991).

Figures

Figure 1. rPrP undergoes LPS under conditions above the binodal curve

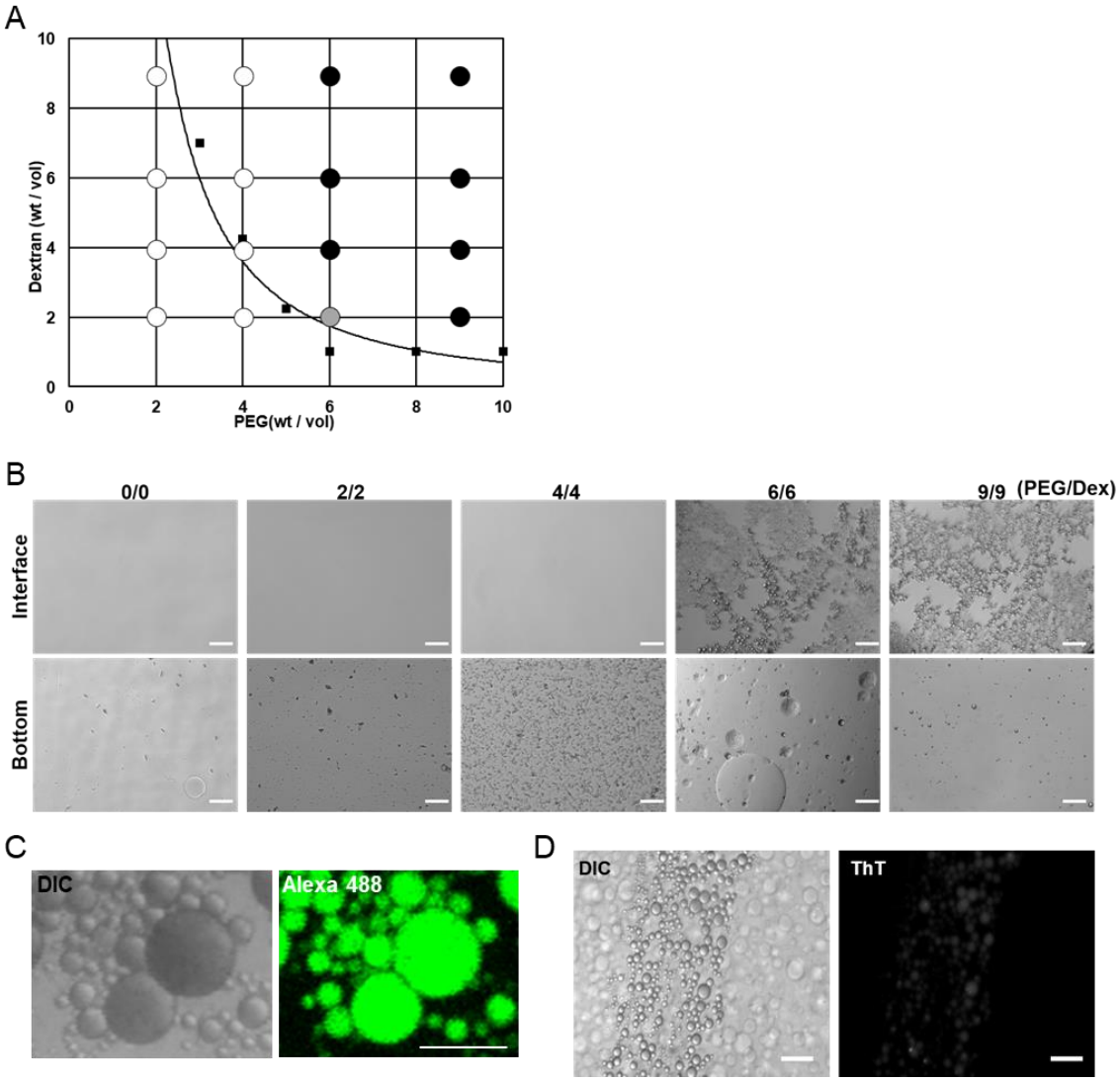

(A) Phase diagram of ATPS and plotting of rPrP at each concentration of polymers with 120 mM sodium thiosulfate ($Na_2S_2O_3$) and 10 µM rPrP (square dots: average of clouding point; solid line: approximation of the binodal curve of PEG/dextran (R^2 = 0.8626); black dots: rPrP fully underwent LPS; gray dots: rPrP underwent LPS but also formed aggregation; white dots: rPrP fully aggregated). (B) Differential interference contrast (DIC) microscopy images of droplet formation at the interface of PEG/dextran solution and bottom of the well after incubation at 37°C for 1 h. Amorphous aggregation precipitated in 0–4% (w/v) of each polymer (PEG/dextran), whereas droplets precipitated at the bottom of the well under conditions above the binodal curve. Bar: 50 µm. (C) Confocal microscopy images of rPrP droplets with Alexa 488-labeled rPrP (1:18). Bar: 20 µm. (D) DIC and fluorescence microscopy images with 50 µM ThT, immediately after mixing the polymer and protein solution. Bar: 50 µm. All experiments were performed under the conditions of 9% (w/v) of each polymer (PEG/dextran), 120 mM $Na_2S_2O_3$, and 10 µM rPrP.

Figure 2. Analysis of liquidity of the droplets of rPrP

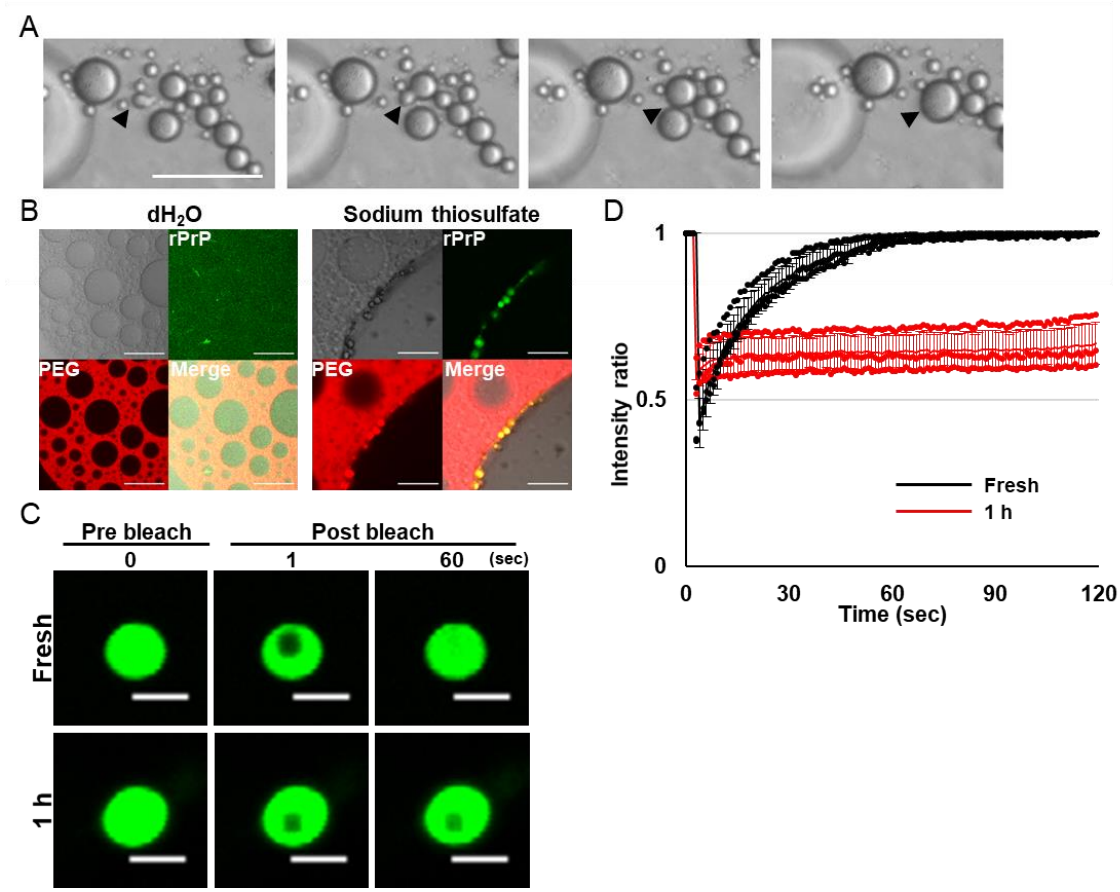

(A) Consecutive images from DIC microscopy of droplets seamlessly combining with each other. Black arrowhead indicates a droplet uniting with another one. (B) Confocal microscopy images of the distribution of PEG (0.01% Rhodamine-PEG: red) and rPrP (1:18 of Alexa488-labeled rPrP: green). Left panel: ATPS solution with dH_2O. Bar: 200 µM. Right panel: ATPS solution with 120 mM sodium thiosulfate ($Na_2S_2O_3$). Bar: 100 µm. Both images were immediately taken after mixing the polymer and protein solution. (C) Confocal microscopy images from FRAP experiment of a fresh (0 min) droplet (top) and a droplet incubated for 1 h (bottom). Bar: 5 µm. (D) Recovery of fluorescence intensity of droplets taken from the FRAP experiment. Black: fresh droplets. Red: droplets incubated for 1 h. Each dot indicates a value measured in three independent experiments. Line indicates the average of the experiments. Bar: SD. N = 3. All experiments were performed under the conditions of 9% (w/v) of each polymer (PEG/dextran), 120 mM $Na_2S_2O_3$ or dH_2O, with 10–13 µM rPrP.

Figure 3. The N-terminal of PrP is essential for droplet formation and maturation

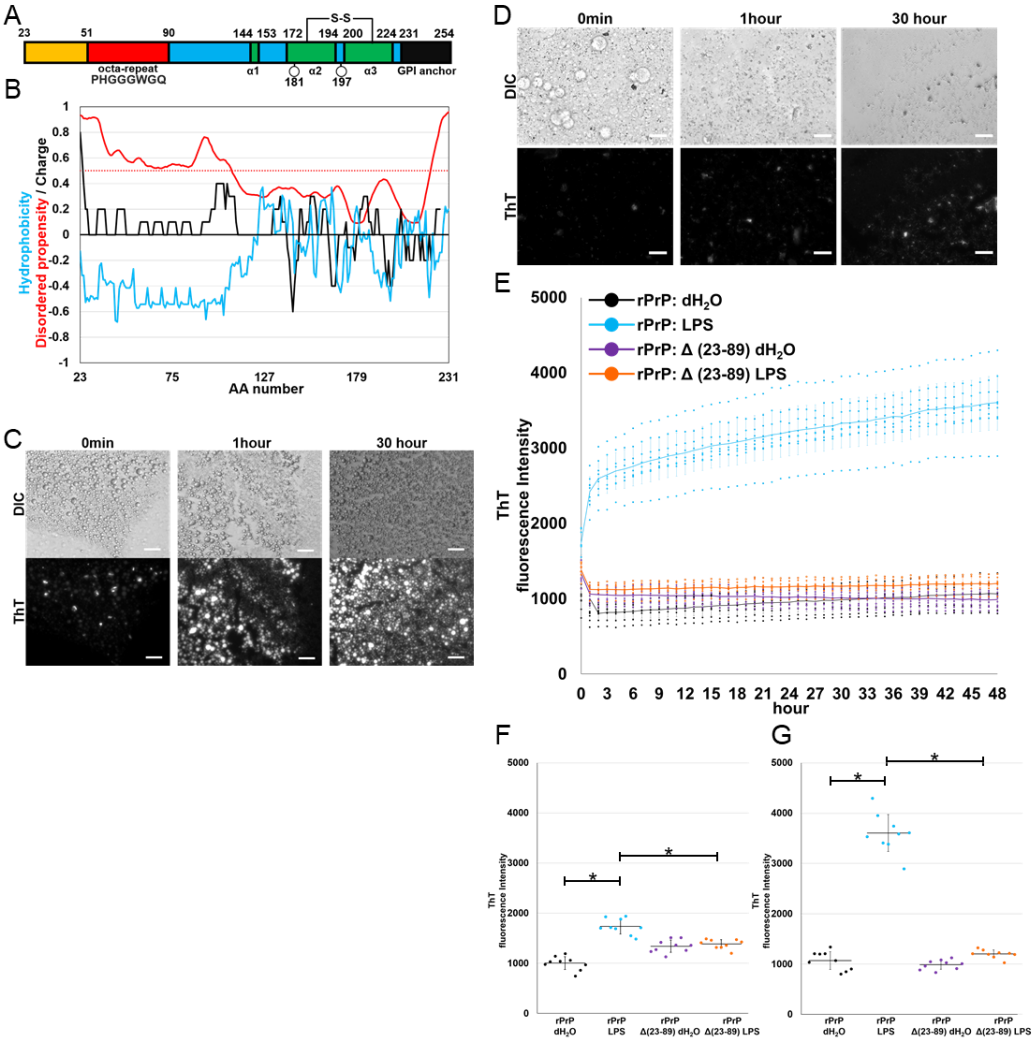

(A) Schematic image of human PrP residues 23–231. Red: octa-peptide region. Green: α-helix regions. Circles: glycosylation site. (B) Calculation of hydrophobicity, disordered propensity, and electric charge of human PrP using Protscale, PrDOS, and EMBOSS. Blue line: hydrophobicity calculated by Protscale. Black line: electric charge calculated by EMBOSS. Red line: disordered propensity calculated by PrDOS. Red dotted line: threshold of disordered propensity (FP: 5%). (C) DIC and fluorescence microscopy images of rPrP: LPS at each time point. Even very small droplets (<5 µm) with no apparent ThT fluorescence at 0 min could be clearly identified after 30 h of incubation. (D) DIC and fluorescence microscopy images of rPrP Δ (23–89): LPS at each time point. (E) ThT fluorescence intensity of rPrP and rPrP Δ (23–89) measured at 48 h. Each dot represents a value measured in three independent experiments. Line indicates the average of each group. (F) Quantification of ThT fluorescence intensity at 0 min. (G) Quantification of ThT fluorescence intensity measured at 48 h. In the "LPS" conditions, experiments were performed under the conditions of 9% (w/v) of each polymer (PEG/dextran), 120 mM sodium thiosulfate, and 10 µM rPrP. In the "dH_2O" conditions, experiments were performed under the conditions of 9% (w/v) of each polymer (PEG/dextran) and 10 µM rPrP without salt. *P < 0.0005. Bar: SD. N = 9. Statistical analysis was performed with one-way ANOVA, followed by Tukey–Kramer test.

Figure 4. Biochemical analysis of gels from rPrP

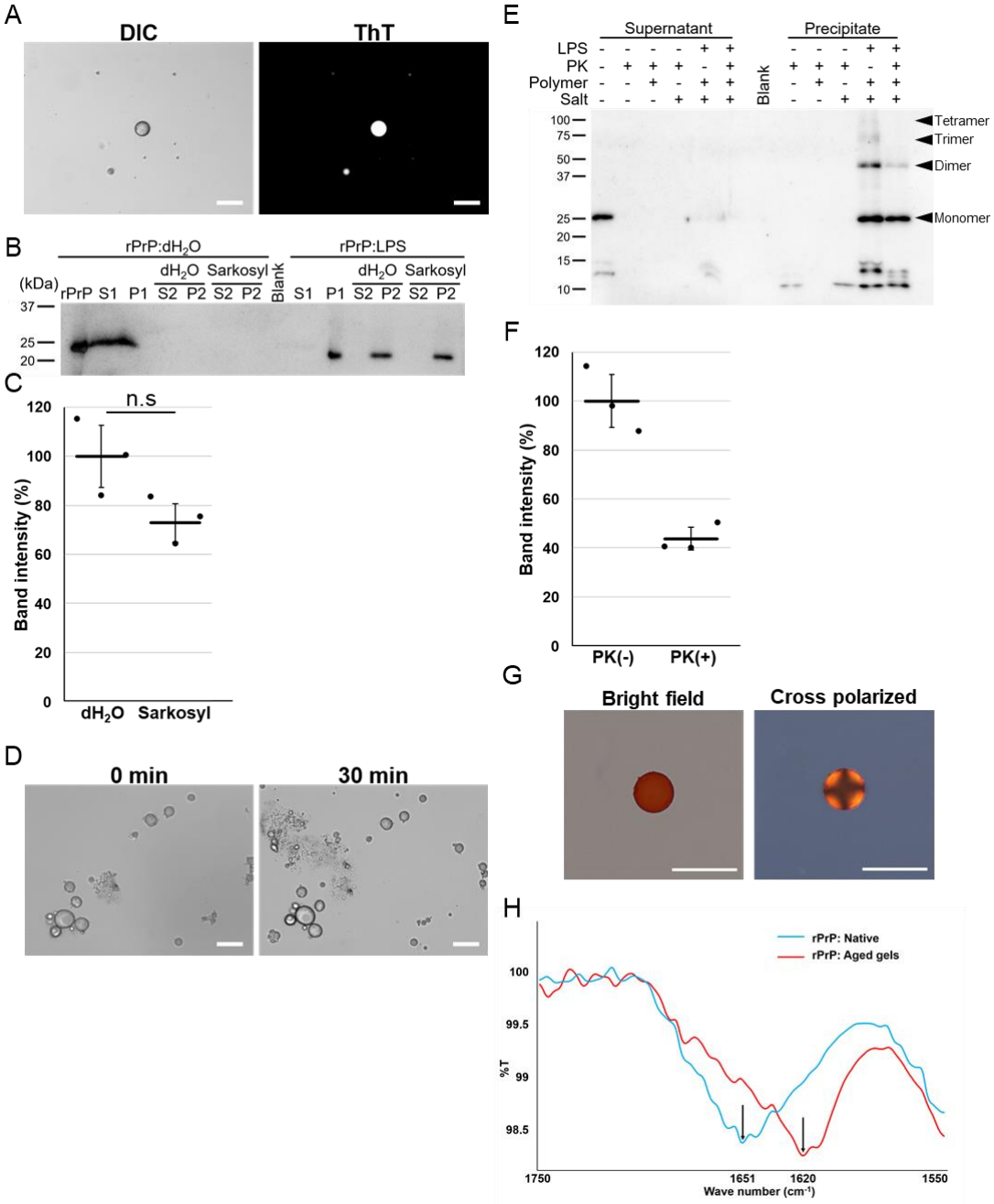

(A) DIC and fluorescence microscopy images of rPrP gel incubated for 30 min in ATPS, collected by centrifugation, and then applied to dH_2O with 50 µm ThT. Bar: 50 µm. (B) Western blotting of rPrP with or without sarkosyl treatment. S1 and P1 were originally collected by centrifugation from the sample diluted with dH_2O. S2 and P2 were collected from the P1 fraction treated with dH_2O or sarkosyl. (C) Quantification of band intensity from the P2 fraction of dH_2O compared with sarkosyl treatment (refer to Fig. 4B). (D) DIC microscopy images of aged gels before (0 min) and after (30 min) PK treatment. (E) Quantification of band intensity of aged gels with or without PK treatment (refer to Fig. 4D). (F) Western blotting of rPrP aged gels. “LPS” indicates that experiments were

performed under the conditions of 9% (w/v) of each polymer (PEG/dextran), 120 mM sodium thiosulfate ($Na_2S_2O_3$), and 10 μM rPrP. “dH_2O” indicates that experiments were performed under the conditions of 9% (w/v) of each polymer (PEG/dextran) and 10 μM rPrP without salt. “Polymer” and “Salt” indicate that the samples contain 9% (w/v) of each polymer (PEG/dextran) and 120 mM $Na_2S_2O_3$. “PK” indicates that samples were treated with 7.5 μg/ml PK. Each dot represents a value measured from an individual sample. Solid line indicates the average. Bar: SD. N = 3. Statistical analysis was performed with unpaired t-tests. “n.s.” means no significant difference. (G) Confocal microscopy images of aged gels stained with Congo red in bright field and cross-polarized. Bar: 50 μm. (H) FTIR spectroscopic analysis of aged gels and native rPrP. Blue line: native rPrP. Red line: Aged gels from rPrP incubated at 37°C for 72 h. Arrows indicate the peak of each sample.

Figure 5. Hypothetical model for the droplet maturation of prion protein

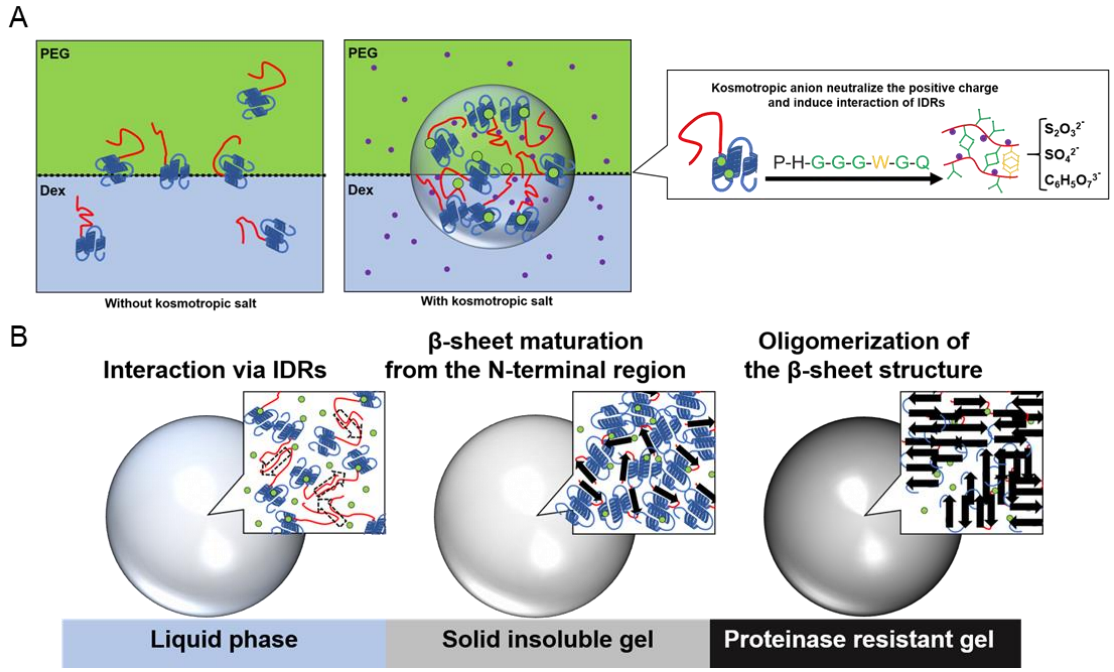

(A) Left: Prion protein molecules are equally distributed in PEG and dextran fractions without kosmotropic anions. Middle: Prion protein molecules assemble each other via IDRs and form droplets at the interface of ATPS by adding kosmotropic anions. Right: Possible interaction inside droplets; PEG may bind to prion protein but with no change in its structure. Kosmotropic anions neutralize the positive charge of IDRs and induce interaction between IDRs (octapeptide repeat at the N-terminal region). Dipole–dipole interaction (green) of glycine (G) and glutamine (Q), and π–π interaction (yellow) of tryptophan (W) are expected to underlie in phase separation and transition. [refer to (41)]. (B) Hypothetical model of droplet maturation. Fresh droplets are composed of native prion protein molecules interacting via IDRs. IDRs may construct a short β-sheet structure [refer to (37)]. As the droplet matures, β-sheet conversion is initiated from IDRs, forming an insoluble gel. Finally, the entire molecule is converted to a β-sheet structure and oligomerized, resulting in proteinase-resistant gel. Yellow green: PEG fraction and PEG molecule. Light blue: Dextran fraction. Red: IDRs of rPrP. Dark blue: constructed region of rPrP including three α-helices. Purple dots: kosmotropic anions. Arrows: β-sheet structure.